A coarse-grained model for a nanometer-scale molecular pump

Oded Hod and Eran Rabani*

School of Chemistry, The Sackler Faculty of Exact Sciences, Tel Aviv University, Tel Aviv 69978, Israel

Communicated by Joshua Jortner, Tel Aviv University, Tel Aviv, Israel, September 25, 2003 (received for review March 31, 2003)

A theory for a nanometer-scale pump based on the ratchet concept is presented. A lattice gas model with a set of moves that satisfy hydrodynamic equations is used to describe an asymmetric nanometer channel connecting two reservoirs of fluid. The channel, which is coupled to an external oscillatory (or stochastic) driving force, pumps fluid from one reservoir to the other. The frequency of the external driving force, the fluid density, and the channel dimensions are used to control the fluid flow. We observe a nonmonotonic behavior of the flow with respect to some model parameters and discuss the efficiency of the device.

Matter confined in nanometer-scale channels has been the subject of numerous theoretical studies over the past decade (1–4). Much of the theoretical attention has been given to the drying transition that occurs in confined water (5–7), with strong connection to biological channels. Intuition would lead one to assume that water confined in hydrophobic channels is unfavorable, and as a result of the reduction of the number of hydrogen bonds compared with the bulk fluid the density of water inside a hydrophobic channel would be very low. Apparently this is not the case as shown recently by Hummer *et al.* (8) and Maibaum and Chandler (9).

Currently we have a good understanding of the phase behavior of liquid confined in nanometer-scale channels. Hummer *et al.* (8) used molecular dynamics simulation to study the density fluctuation of water inside a single-wall carbon nanotube as a model for a hydrophobic channel. Their results were rationalized by a simple coarse-grained model developed by Maibaum and Chandler (9), who showed that the occupation number inside the hydrophobic channel depends mainly on the ratio of solvent–solvent interaction strength to solvent–tube interaction strength, in agreement with the molecular dynamics simulations. In contrast, there is still a debate regarding the dynamics of emptying or filling the channel (8–11). Hummer *et al.* (8) and Beckstein *et al.* (11) argued that water flow through the nanotube occurs in bursts. On the other hand, the simple lattice gas approach indicates that the bursts arise from the definition of a conductance event (9).

The major goal of the present study is to develop a useful approach to control the flow of a fluid (water, for example) through a confined channel. In contact with the aforementioned studies the only (well supported) assumption made is that the density of the fluid confined in the channel can be controlled by adjusting the relevant interactions (8, 9). The mechanism by which transport occurs, i.e., the mechanism of emptying or filling the channel is of minor importance for the present application.

To illustrate how one can control the flow of a fluid through a channel we focus on a simple model system where a channel connects two reservoirs of fluid. Following the work of Maibaum and Chandler (9), we use a coarse-grained lattice gas model on a triangular lattice to describe the system. The dynamics of the fluid are approximated by the Frisch–Hasslacher–Pomeau (FHP) model (12, 13) with a set of moves that satisfy the Navier–Stokes equation (14). We assume that the fluid can wet the inside of the channel and use no-slip boundary conditions to model the couplings between the fluid and the nanotube and between the fluid and the wall separating the two reservoirs. The geometry of the system and the detailed description of the model are given in *Model*.

We adopt the ratchet concept to control the flow of fluid through the channel (15–19). The basic idea behind the ratchet effect is simple (20). A Brownian particle can undergo net transport on an asymmetric periodic potential energy surface that fluctuates periodically between its different states. In the present study we introduce structural asymmetry along the channel (asymmetric potential) and apply an external periodic force on the channel connecting the two reservoirs. This simple geometry leads to a net transport of fluid from one reservoir to the other despite the fact that it is not periodic.

Similar ratchets have been used in many ways, including for the separation of particles based on diffusion (21–26). Of particular relevance to the present study is the work of Müller and coworkers (24, 25) and Siwy and Fuliński (26). Müller and coworkers (24, 25) showed how a net transport of micrometer-sized particles through a silicon wafer can be tuned by periodically pumping a liquid through the silicon pores. Using an asymmetric, ratchet-like, electric potential inside a conical pore, Siwy and Fuliński (21) synthesized a nano-device that transports potassium ions against their concentration gradient. As will become clear below, our approach combines several important features discussed in refs. 24 and 25 for mesoscopic materials and in ref. 26 for ionic systems.

We use simulation techniques to study the relevant parameters that can be used to control the flow of fluid through the channel. Specifically, we delineate the effects of the frequency of the external driving force, the fluid density, and the dimensions of the channel.

Model

We propose a simple coarse-grained 2D lattice gas model to describe the nanometer channel (for example, a nanotube) that is connected to a wall separating two reservoirs of fluid. A sketch of the model is shown in Fig. 1.

The dynamics of the fluid is described within the FHP-III model based on a triangular grid (13). In the FHP-III model, identical fluid particles travel with unit speed from one site to the other on the grid and collide when they meet on the same site, conserving both particle density and particle momentum. Only one particle is allowed to travel in each direction along the six possible links connecting adjacent sites. Each site can also include a rest particle that can take part in the collision process. The equations of motion can be expressed in terms of a vector, $\mathbf{n}(\mathbf{r}, t) = \{n_0(\mathbf{r}, t), \ldots, n_6(\mathbf{r}, t)\}$, with binary variable components that are proportional to the density of particles moving from site $\mathbf{r}$ in one of the possible directions $\mathbf{c}_j$:

$$n_j(\mathbf{r} + \mathbf{c}_j, t + 1) = n_j(\mathbf{r}, t) + \Delta_j(\mathbf{n}(\mathbf{r}, t)), \qquad [1]$$

where $\mathbf{c}_j = (\cos(2\pi j/6), \sin(2\pi j/6)), j = 1, \ldots, 6$ for the six possible direction, or $\mathbf{c}_j = (0, 0)$ for the rest particle. The collision operator,

Abbreviation: FHP, Frisch–Hasslacher–Pomeau.

*To whom correspondence should be addressed. E-mail: rabani@tau.ac.il.

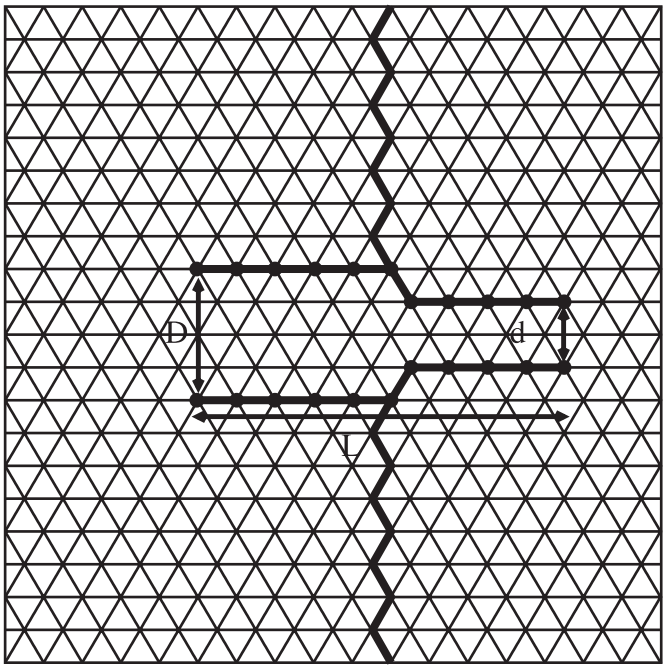

Fig. 1. A sketch of the triangular grid used in our lattice gas model. There are six links connecting each site to its neighbors. The sites of the channel are labeled by full circles connected by the thick solid line. The wall separating the two reservoirs is labeled by a thick solid line. The diameter of the wide and narrow ends of the channel is given by *D* and *d*, respectively, and the length of the channel is given by *L*.

$\Delta_j(\mathbf{n}(\mathbf{r},t))$, includes 76 possible two-, three-, four-, and five-particle collisions. We also include straightforward higher order collisions. These collisions conserve mass $\Sigma_j\Delta_j(\mathbf{n}(\mathbf{r},t)) = 0$ and momentum $\Sigma_j\mathbf{c}_j\Delta_j(\mathbf{n}(\mathbf{r},t)) = 0$ and are described elsewhere (14).

The channel is introduced to the model by labeling certain lattice sites and introducing different collision rules at these sites. The choice of the asymmetric structure of the channel studied in this work is shown in Fig. 1. The channel sites are labeled by black circles connected by a thick solid line. The diameter of the wide (D) and narrow (d) ends, and the length of the channel (L) are also shown in Fig. 1. We use no-slip conditions at the boundaries by forcing any particle colliding with the channel to return along the link on which it approached the channel (27). We apply similar collision rules between the fluid particles and the wall separating the two reservoirs. The walls are labeled by the thick solid line in Fig. 1.

We start from a random initial configuration of fluid on the lattice with uniform density (unless otherwise noted),[†] at each reservoir. The propagation in time involves the following three steps: (*i*) a collision step, (*ii*) a travel step, and (*iii*) a channel movement step arising from the external driving force, with a period ω. The details are as follows:

(*i*) At each time step particles at all sites collide according to the rules specified above and in ref. 14. These include particle–particle, particle–channel, and particle–wall collisions.

(*ii*) After the collision step each particle travels in a straight line along one of the lattice links (according to its velocity vector), unless it is a rest particle, until it arrives to the next site.

(*iii*) The channel movement step arising from the applied external force is slightly more involved. First, we apply collision rules at the predicted new sites of the channel. Particles are not allowed to penetrate the channel through the walls or move along the boundaries of the wall. An example for a single collision of a particle moving along direction C_j before the collision, and along direction C'_j after the collision ($C_j \rightarrow C'_j$), with the upper wall moving to the right is given by: {E→E; SE→E; SW→NE; W→E; NW→NE; NE→NE; stationary→E}, where N, S, E, and W stand for north, south, east, and west directions, respectively. If after the collision with the walls of the channel a link is occupied with more than a single particle, the excess particles are propagated along their new direction. This procedure is repeated until all links with excess particles are occupied by not more than a single particle. After this step we move each channel site along a straight line in the direction of the external force until it arrives to the next site, preserving the structure of the channel.

Results and Discussion

To study the fluid dynamics through the channel we have performed simulations based on the lattice gas approach described above for different model parameters. The effects of the dimensions of the channel (diameters d, D, and length L), the frequency of the external driving force (ω, defined as the reciprocal time for one full cycle), and the density of the fluid on the flow were studied in detail. We have used $N_{grid} = 500{,}000$ lattice sites, unless otherwise stated, and imposed periodic boundary condition at the grid edge perpendicular to the channel axis. No-slip (reflection) boundary conditions were imposed at the remaining edge, unless otherwise noted. Each propagation step included a full cycle of the three steps described in *Model*. The propagation was stopped after the system approached its steady-state solution.

In Fig. 2 we show a snapshot of the velocity field at each site averaged over the initial 1,000 time steps. The frequency of the external force is $\omega = 0.1$ (in units of reciprocal propagation steps), the density of the fluid is $\rho = 0.5$, the diameters of the narrow and wide ends are $d = 5$ and $D = 11$ lattice sites, respectively, and the total length is $L = 20$ lattice sites. A net flow of fluid through the channel from the narrow end to the wide end, as indicated by the directions of the arrows, is clearly seen.

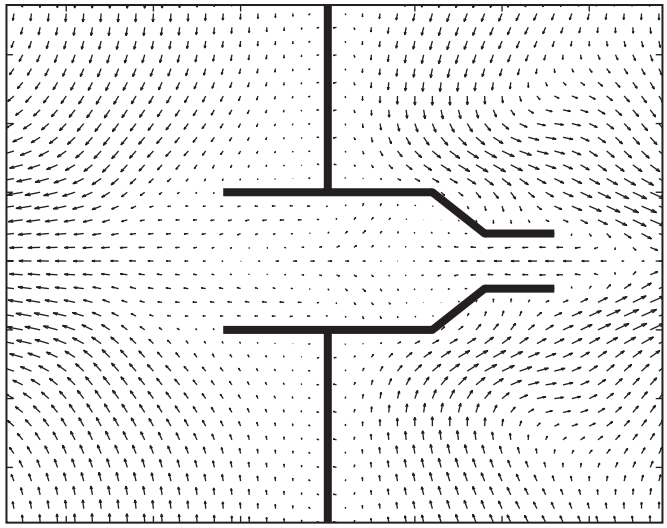

Fig. 2. A snapshot, zoomed in the region of the channel, of the velocity field at each site averaged over 1,000 time steps. The frequency of the external force is $\omega = 0.1$ (in units of reciprocal propagation steps), the density of the fluid is $\rho = 0.5$, and the diameters of the narrow and wide ends are $d = 5$ and $D = 11$ lattice sites, respectively. The arrows indicate the direction of the velocity field at each site. The magnitude of the velocity is proportional to the size of the arrow.

[†]The density $\rho = 1/N_{occ}\Sigma_j n_j$ is defined as the sum over the occupation numbers of the links at each site (n_j) divided by the maximum occupation number at each site (N_{occ}).

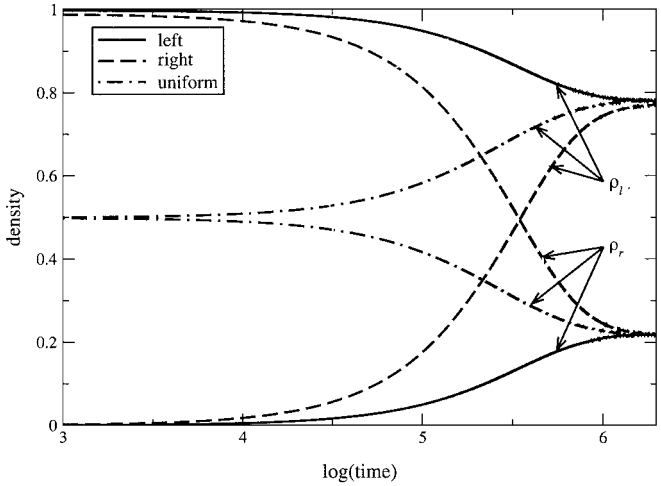

Fig. 3. Plots of the average density in each reservoir versus time on a semilogarithmic scale. The parameters are the same as in Fig. 2. Three different initial conditions are considered: left (solid line), right (dashed line), and uniform (dotted-dashed line) for an initial density in the left reservoir, an initial density in the right reservoir, and a uniform initial density, respectively. All three cases approach the same steady-state solution at long times. At steady state, the density difference between the two reservoirs is nearly 100% of the average density.

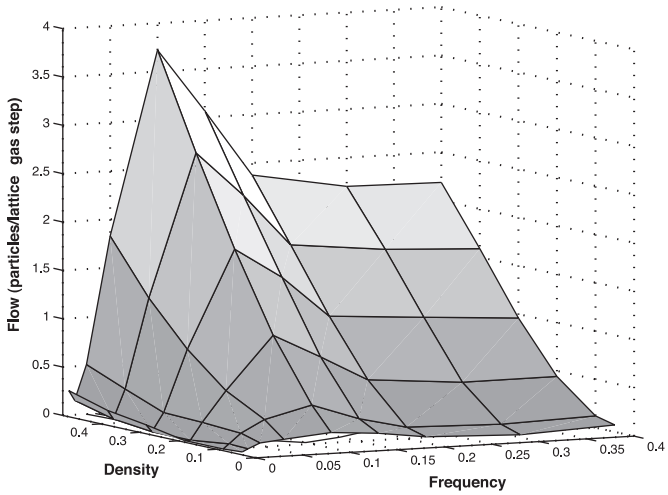

Fig. 4. A 2D plot of the flow versus fluid density (ρ) and frequency of the external oscillatory driving force (ω). Note the pronounced maximum of the flow for a fixed density as a function of ω. The dimensions of the channel are the same as in Fig. 2

The direction of the flow can be traced to the fact that any particle inside the channel placed near the boundary between the narrow and wide ends can only be pushed by the channel in the direction of the wide end. It is interesting to note that the flow is more directional and the current is larger at the narrow side of the channel. Similar behavior is expected for macroscopic channels, where a narrow end is used to increase the current for a given pressure gradient.

Typical kinetics of the time dependence of the average density in each reservoir (ρ_l and ρ_r for the left and right densities, respectively) is shown in Fig. 3 on a semilogarithmic scale. The density, frequency, and other parameters are identical to those of Fig. 2. The buildup of density gradient follows exponential kinetics, with a steady-state solution that is independent of the initial conditions. To illustrate this we have used three different initial conditions that result in the same steady-state solution. As can be seen in Fig. 3, the final fluid density in each reservoir is the same in all three cases. We have also studied the kinetics starting from the steady-state solution and switched off the external oscillatory force (data not shown). Typically, we find that the decay of the density to equilibrium is faster than the buildup of density gradient in the presence of the external driving force.

The fact that the density in each reservoir approaches a steady state is a consequence of the finite size of the system, namely the finite size of the two reservoirs. We find that steady-state densities are independent of the dimensions of the reservoirs; however, the rate of approach to steady state decreases as the dimensions of the system increase. Therefore, a more meaningful observable that is independent of the size of the reservoirs is the average fluid flow through the channel, which can be obtained from the short time dynamics of the density gradient. The magnitude of the flow obtained this way is identical to the flow (at steady state) for infinite reservoirs. (Note that for a finite system the average flow approaches zero at long times.)

A 2D plot of the flow as a function of the density of the fluid (ρ) and the frequency of the external oscillatory force (ω) is shown in Fig. 4. The diameters of the narrow and wide ends are $d = 5$ and $D = 11$ lattice sites, respectively, and the total length is $L = 20$ lattice sites. The flow, J, is calculated from $J = N_{occ}N_{grid}\lim_{t\to 0} d\Delta\rho/dt$, where $N_{occ} = 7$ for the FHP-III model, and $\Delta\rho = \rho_l - \rho_r$ is the average density difference between the two reservoirs (namely, $J \propto d(N_l - N_r)/dt$). This definition of the flow assures that J is independent of grid size. For a given fluid density, a nonmonotonic behavior, with a well pronounced global maximum, is observed for the average flow as a function of ω. At lower values of ω the system has enough time to relax back to the equilibrium state with equal densities at both sides of the channel, so that the net flow is very small. At higher values of ω there is a separation of time scales between the motion of the fluid and the channel. In this limit using a mean field treatment, one finds that the flow through the channel is sensitive to the average position of the channel. This leads to a diminishing net current at higher values of ω. In between these limiting cases the flow is larger, giving rise to a maximum of flow versus ω. In addition, we find that the flow of the liquid through the channel increases with increasing density for all values of ω, as can clearly be seen in Fig. 4.

We have also studied the effects of the dimensions of the channel on the resulting flow and on the density of the fluid in the reservoirs at steady state. The results for a set of simulations of different channel dimensions are summarized in Tables 1 and 2. The particle density is $\rho = 0.5$, and the frequency of the external driving force is $\omega = 0.15$ (in units of reciprocal propagation steps). We observe a maximum value of flow when we increase the width of the wide and narrow ends such that the difference $D - d = 6$ is constant. This is a result of two

Table 1. Values of current (number of particles per time step) and density difference at steady state for different channel dimensions, *d* and *D* (in units of lattice sites)

d	D	J	$\Delta\rho$
3	9	0.61	101%
5	11	3.30	110%
9	15	10.3	50.0%
17	23	18.6	14.8%
31	37	17.5	4.40%
61	67	8.20	1.00%

Note that $D - d = 6$ is constant. The particle density is $\rho = 0.5$, the frequency of the external driving force is $\omega = 0.15$ (in units of reciprocal propagation steps), and the length of the channel is $L = 20$.

PHYSICS

Table 2. Values of current (number of particles per time step) and density difference at steady state for different channel length

L	J	$\Delta\rho$
20	3.30	110%
40	1.85	116%
60	1.17	113%

The particle density is $\rho = 0.5$, the frequency of the external driving force is $\omega = 0.15$ (in units of reciprocal propagation steps), and the width of the channel is $d = 5$ and $D = 11$ lattice sites.

competing effects. On one hand, as the dimensions of the channel increase the pressure gradient required for fluid flow decreases (28). But at the same time, the efficiency of the pump reduces with increasing dimensions, giving rise to a maximum of flow at an intermediated channel width. Unlike the nonmonotonic behavior observed for the fluid flow, the difference in fluid densities ($\Delta\rho$) at steady state decreases monotonically (within the statistical noise) with the diameters of the channel.

We have also studied the effects of increasing the length of the channel on the fluid current and on $\Delta\rho$ at steady state. We find that increasing the length of the channel always results in a decrease in the fluid flow (see Table 2). We have tripled the length of the channel from 20 to 60 lattice sites. Within this range fluid current decreases linearly with the length of the channel. On the other hand, increasing the size of the channel has a negligible effect on the steady-state fluid densities at each reservoir.

So far we have discussed the properties of our nanopump in terms of its reduced lattice-gas dimensions. To make connections to a realistic system we have calculated the Reynolds number for several simulation cases and used the definition of this number to provide values for the relevant control parameters. The Reynolds number, R_e, is given by

$$R_e = \frac{ud}{\nu}, \qquad [2]$$

where u is the average fluid velocity in the pump region and is proportional to $u \propto A\omega$, where as before ω is the frequency of the external force and A is its amplitude. In the above equation, d is the diameter of the pump and ν is the kinematic viscosity of the fluid. Thus, for a given fluid kinematic viscosity, and for a given channel dimension, we can estimate the frequency of the driving force, or vice versa.

For the FHP-III lattice gas model we have used the following definitions to calculate the Reynolds number. The time averaged velocity field is given by

$$\mathbf{u}(\mathbf{r}) = \frac{\sum_{i=0}^{6} \mathbf{c}_i N_i(\mathbf{r})}{\sum_{i=0}^{6} N_i(\mathbf{r})}, \qquad [3]$$

where $N_i(\mathbf{r})$ is the mean occupation number calculated as a time average of the occupation number $n_i(\mathbf{r}, t)$ defined above. The (scaled) kinematic viscosity is given by (29)

$$\nu = \frac{\frac{1}{28}\frac{1}{\rho(1-\rho)}\frac{1}{1-8\rho(1-\rho)/7} - \frac{1}{8}}{\frac{7}{12}\frac{1-2\rho}{1-\rho}}. \qquad [4]$$

The results for the Reynolds numbers for different simulation conditions are summarized in Table 3. In these simulations we have used periodic boundary conditions in both the longitudinal and transverse directions. The Reynolds number increases monotonically with the dimensions of the channel. The values obtained for the Reynolds number fall in intermediate range (0.06−7.2) for the densities and channel dimensions studied. These values correspond to a frequency of the external driving force in the range of $\omega \approx 0.5-50$ GHz for liquid water (kinematic viscosity $\nu = 10^{-6}\cdot m^2\cdot s^{-1}$), for pump diameter of $d = 10$ nm and oscillation amplitude of $A = 10$ nm. Clearly, smaller pump frequencies are required for smaller Reynolds numbers or larger channel dimensions. We have also studied the effects of increasing the amplitude of oscillation, A. A sublinear increase of the Reynolds number with A was observed, indicating that larger amplitudes would also lead to lower frequencies of the driving force. It is interesting to note that gigahertz oscillators based on the motion of the inner shell of a multiwall carbon nanotube have been discussed recently (30). This system maybe useful as a building block for a nanometer-scale pump based on the concepts introduced above.

Table 3. Values of the average velocity within the pump (in lattice-gas units) and the Reynolds number at steady state for different channel dimensions, d and D (in units of lattice sites) and densities ρ

ρ	D	d	$\langle u \rangle$	R_e
0.05	11	5	0.027	0.11
0.05	23	17	0.045	0.63
0.05	37	31	0.032	0.82
0.25	11	5	0.018	0.30
0.25	23	17	0.099	5.57
0.25	37	31	0.070	7.20
0.45	11	5	0.009	0.06
0.45	23	17	0.141	3.34
0.45	37	31	0.087	3.73

The frequency of the external driving force is $\omega = 0.05$ (in units of reciprocal propagation steps), the length of the channel is $L = 20$ lattice sites, and the oscillation amplitude is $A = 5$ lattice sites.

Conclusions

A simple asymmetric geometry of a nanometer-scale channel connecting two reservoirs of fluid, coupled to an external periodic or stochastic driving force, can be used to pump material on a nanometer-length scale. The rate of flow through the device depends on the fluid density, the frequency and amplitude of the external force, and the dimensions of the channel.

We have developed a simple coarse-grained lattice gas model with FHP fluid dynamics that satisfy the Navier–Stokes equation to study the dynamic flow of fluid through a nanometer channel. The only well supported assumption made is that the fluid can wet the inside of the channel. Using simulation techniques we have studied the flow through the channel for different model parameters.

We showed that the flow is a nonmonotonic function of the frequency of the external force (ω) and the diameters of the channel. At low and high values of ω the fluid current through the channel is very small, whereas in between these limiting cases the flow is higher, giving rise to a maximum of flow at finite ω. Because of the competition between the pump efficiency and the pressure gradient required to push the fluid through the channel, a maximum in the current was also observed when the dimensions of the channel were increased. On the other hand, a monotonic behavior was observed for the fluid current with respect to fluid density and length of the channel.

We thank Profs. Michael Urbakh and Joseph Klafter for valuable discussions. O.H. thanks Prof. Israel Hod and Dr. Sergey Denysov for stimulating discussions. This work was supported by the Israel Science Foundation founded by the Israel Academy of Sciences and Humanities.

1. Prigogine, I. & Rice, S. A., eds. (1988) *Advances in Chemical Physics* (Wiley, New York), Vol. LXXI.
2. Karplus, M. & Petsko, G. A. (1990) *Nature* **347,** 631–639.
3. Roux, B. (1999) *Biophys. J.* **77,** 139–153.
4. Dellago, C., Naor, M. M. & Hummer, G. (2003) *Phys. Rev. Lett.* **90,** 105902.
5. Wallqvist, A. & Berne, B. J. (1995) *J. Phys. Chem.* **99,** 2893–2899.
6. Lum, K. & Luzar, A. (1997) *Phys. Rev. E* **56,** R6283–R6286.
7. Lum, K., Chandler, D. & Weeks, J. D. (1999) *J. Phys. Chem. B* **103,** 4570–4577.
8. Hummer, G., Rasiah, J. C. & Noworyta, J. P. (2001) *Nature* **414,** 188–190.
9. Maibaum, L. & Chandler, D. (2002) *J. Phys. Chem. B* **107,** 1189–1193.
10. Berezhkovskii, A. & Hummer, G. (2002) *Phys. Rev. Lett.* **89,** 064503.
11. Beckstein, O., Biggin, P. C. & Sansom, M. S. P. (2001) *J. Phys. Chem. B* **105,** 12902–12905.
12. Frisch, U., Hasslacher, B. & Pomeau, Y. (1986) *Phys. Rev. Lett.* **56,** 1505–1508.
13. Frisch, U., d' Humiéres, D., Hasslacher, B., Lallemand, P. & Pomeau, Y. (1987) *Complex Systems* **1,** 649–707.
14. Rothman, D. H. & Zaleski, S. (1994) *Rev. Mod. Phys.* **66,** 1417–1479.
15. Reimann, P. (2002) *Phys. Rep.* **361,** 57–265.
16. Hänggi, P. & Bartussek, R. (1996) in *Lecture Notes in Physics*, eds. Parisi, J, Müller, S. C. & Zimmermann, W. (Springer, Berlin) Vol. 476, pp. 294–308.
17. Astumian, R. D. (1997) *Science* **276,** 917–922.
18. Jülicher, F., Ajdari, A. & Prost, J. (1997) *Rev. Mod. Phys.* **69,** 1269–1281.
19. Astumian, R. D. & Hanggi, P. (2002) *Phys. Today* **55,** 33–39.
20. Bug, A. L. R. & Berne, B. J. (1987) *Phys. Rev. Lett.* **59,** 948.
21. Rousselet, J., Salome, L., Ajdari, A. & Prost, J. (1994) *Nature* **370,** 446–448.
22. Faucheux, L. P., Bourdieu, L. S., Kaplan, P. D. & Libchaber, A. J. (1995) *Phys. Rev. Lett.* **74,** 1504–1507.
23. Bader, J. S., Hammond, R. W., Henck, S. A., Deem, M. W., McDermott, G. A., Bustillo, J. M., Simpson, J. W., Mulhern, G. T. & Rothberg, J. M. (1999) *Proc. Natl. Acad. Sci. USA* **96,** 13165–13169.
24. Kettner, C., Reimann, P., Hänggi, P. & Müller, F. (2000) *Phys. Rev. E* **61,** 312–323.
25. Matthias, S. & Müller, F. (2003) *Nature* **424,** 53–57.
26. Siwy, Z. & Fuliński, A. (2002) *Phys. Rev. Lett.* **89**, 198103.
27. Cornubert, R., d'Humiéres, D. & Levermore, D. (1991) *Physica D* **47,** 241–259.
28. Moseler, M. & Landman, U. (2000) *Science* **289,** 1165–1169.
29. Wolf-Gladrow, D. A. (2000) *Lattice-Gas Cellular Automata and Lattice Boltzmann Models* (Springer, New York).
30. Zheng, Q. & Jiang, Q. (2002) *Phys. Rev. Lett.* **88,** 045503.